Journal of Solid State Chemistry 182 (2009) 2613–2619

Contents lists available at ScienceDirect

Journal of Solid State Chemistry

journal homepage: www.elsevier.com/locate/jssc

Slater–Pauling behavior within quaternary intermetallic borides of the $Ti_3Co_5B_2$ structure-type

Jens Burghaus [a], Richard Dronskowski [a,*], Gordon J. Miller [b]

[a] Institute of Inorganic Chemistry, RWTH Aachen University, Landoltweg 1, 52062 Aachen, Germany
[b] Department of Chemistry, Iowa State University, Ames, IA 50011, USA

ARTICLE INFO

Article history:
Received 1 May 2009
Received in revised form
1 July 2009
Accepted 12 July 2009
Available online 17 July 2009

Keywords:
Itinerant magnetism
Density-functional theory
Chemical bonding
Borides
Intermetallics

ABSTRACT

First-principles, density-functional studies of several intermetallic borides of the general type $M_2M'Ru_{5-n}Rh_nB_2$ ($n = 0$–5; M = Sc, Ti, Nb; M' = Fe, Co) show that the variation in saturation magnetic moment with valence-electron count follows a Slater–Pauling curve, with a maximum moment occurring typically at 66 valence electrons. The magnetic moments in these compounds occur primarily from the 3*d* electrons of the magnetically active M' sites, with some contribution from the Ru/Rh sites via magnetic polarization. Electronic DOS curves reveal that a rigid-band approach is a reasonable approximation for the estimation of saturation moments and the analysis of orbital interactions in this family of complex borides. COHP analyses of the M'–M' orbital interactions indicate optimized interactions in the minority spin states for Co-containing phases, but strong bonding interactions remaining in Fe-containing phases.

1. Introduction

During the last decade, the search for novel intermetallic magnets with potentially anisotropic or low-dimensional magnetic behavior has resulted in the discovery of quaternary metal-rich borides adopting the $Ti_3Co_5B_2$ structure-type with the general formula $M_2M'T_5B_2$ (M = Mg or Sc; M' = main-group metal, e.g., Be, Al, Si, or a 3*d* element; T = Ru, Rh, Ir) [1–4]. Among these compounds, those containing magnetically active 3*d* elements are of special interest because they exhibit long-range magnetic ordering, viz., ferromagnetic or antiferromagnetic behavior. Both experimental and theoretical investigations have revealed exceptional magnetic properties of this series of compounds [4], offering potential applications for data storage and retrieval.

Among the transition metals, only Fe, Co, and Ni exhibit ferromagnetism at room temperature [5]. In these elements the valence 3*d* electrons are the carriers of magnetism, electrons which occupy orbitals that form energy bands with the bands of the valence 4*s* and 4*p* orbitals of the metal. Since these elements have an incomplete 3*d* subshell, occupation according to Pauli's exclusion principle and Hund's rule (maximum spin multiplicity) creates holes in this subshell, the numbers of which are equal to the saturation magnetic moment. Under the reasonable assumption that these 3*d* electrons also participate in chemical bonding [5], the saturation moment is even lower than expected. Hence, Fe, Co, and Ni exhibit saturation moments of 2.22 μ_B (Fe), 1.72 μ_B (Co) and 0.62 μ_B (Ni) at 0 K [6]. This result for the 3*d* metals is based on two bands of electronic states, overlaying each other in energy. One of these is the low, broad conduction band, showing an almost free-electron energy distribution, which originates from the 4*s* and 4*p* orbitals, and the second is the narrower band, lying somewhat higher in energy than the bottom of the conduction band, which is derived from the 3*d* orbitals.

For simple alloys of the 3*d* metals based on fcc and bcc structures, the evolution of the saturation magnetic moment as a function of band filling by the valence 4*s* and 3*d* electrons can be described by a so-called Slater–Pauling curve [7,8]. In this curve, the saturation magnetic moment per atom is plotted vs. valence-electron count per atom, and it exhibits a volcano-shaped plot [9,10], which does show deviations that can be attributed to structural instabilities as well as changes in collinear ordering of local magnetic moments [11]. Nevertheless, the Slater–Pauling curve provides a qualitative assessment of the relationship between itinerant magnetism and band filling in 3*d* systems, and has shown applicability to intermetallic systems, e.g., the Laves phases $Dy(T, T')_2$ (T, T' = Mn, Fe, Co) [12,13] as well as the Heusler alloys Mn_2FeZ (Z = Al, Ga, Si, Ge, Sb) and $Cr_{2-x}Co_{1+x}Al$ [14,15]. The present publication discusses the dependency of saturation magnetic moments on valence-electron count (VEC) for the complex, quaternary intermetallic borides $M_2M'T_5B_2$ and the possibility of a Slater–Pauling relationship.

All quaternary intermetallic borides mentioned above are based on the general chemical composition $M_2M'Ru_{5-n}Rh_nB_2$, in which the Ru and Rh contents can be continuously varied in the

* Corresponding author.
E-mail address: drons@HAL9000.ac.rwth-aachen.de (R. Dronskowski).

0022-4596/$ - see front matter © 2009 Elsevier Inc. All rights reserved.
doi:10.1016/j.jssc.2009.07.017

region $n = 0$–5. Among these compounds, those which exhibit ferromagnetic behavior turned out to have at least 65 valence electrons (e.g., $Sc_2FeRh_5B_2$) [4]. Analyses of the non-spin-polarized electronic structures by crystal orbital Hamilton population (COHP) [16] identified antibonding 3*d* metal–3*d* metal orbital interactions at the Fermi level, whereas antiferromagnets (e.g., $Mg_2MnRh_5B_2$) have a maximum of 62 valence electrons and corresponding non-bonding 3*d*–3*d* interactions at the Fermi level [4]. There is no quantitative rule yet for the magnetic properties of those compounds which exhibit a VEC of 63 or 64 electrons.

Recent theoretical and also experimental results within the series $Sc_2FeRu_{5-n}Rh_nB_2$ [17,18] indicated an increase of the saturation magnetic moment as the Rh content increases and concludes at a maximum saturation moment for $Sc_2FeRh_5B_2$ (VEC = 66). Any effects due to varying the VEC in this region were experimentally investigated by adjusting the chemical composition due to substitution of *M* and *M′* within $M_2M'Ru_{5-n}Rh_nB_2$ by suitable elements. For the present theoretical study, only Fe and Co were chosen as magnetically active elements *M′*, since Ni has a very low magnetic moment at room temperature. Additionally, alkaline earth and early transition metals with s^2 up to s^2d^3 gas phase electronic configurations, e.g., realized in Sc, Ti, and Nb, for *M* were used to adjust the VEC of this series in the target region of about 60–69 valence electrons.

2. Crystal structure and computational details

As mentioned above, all quaternary intermetallic borides with the general formula $M_2M'T_5B_2$ crystallize in an ordered substitutional variant of the $Ti_3Co_5B_2$ aristotype [17] with space group *P*4/*mbm*. Fig. 1 shows a perspective view along the *c*-axis of the tetragonal structure of $M_2M'T_5B_2$. The *T* atoms, which are Ru, Rh, or a mixture of these two elements, form a robust framework constructed of trigonal prisms, tetragonal prisms (pseudo-cubes), and pentagonal prisms with *M*, *M′*, and B atoms occupying the voids: the trigonal prisms by B atoms; the tetragonal prisms by the magnetically active *M′* atoms; and the pentagonal prisms by *M* atoms. Of special interest for the magnetic properties, in particular, are the one-dimensional wires (along *c*) of the magnetically active element *M′*, e.g., Fe, Co, Ni, shown in red.

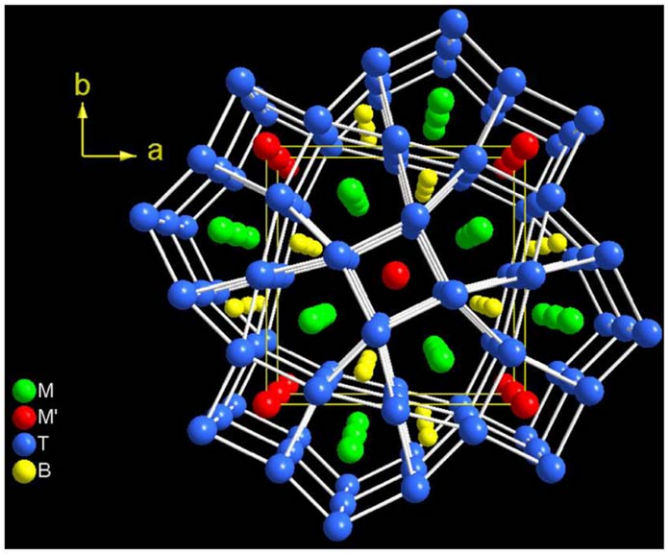

Fig. 1. A view along the *c*-axis into the tetragonal $M_2M'T_5B_2$ structure; see also text.

Theoretical determination of the structural and electronic properties were carried out using the Vienna *ab-initio* simulation package (*VASP*) [19–21], based on density functional theory (DFT) using plane-wave basis sets. Projector-augmented-wave (PAW) potentials were used [22,23], describing the exchange-correlation potential with the generalized gradient approximation (GGA) parameterized by Perdew and Wang [24]. A $4 \times 4 \times 16$ Monk-horst–Pack [25] *k*-point grid referring to one unit cell containing two formula units was used for integrations within the Brillouin zone. Spin-polarized calculations were performed with integer starting values for all local magnetic moments, namely 3 for all magnetically active elements and 0 for all other elements. Forces, stress tensors, atomic positions, unit cell shapes, and unit cell volumes of the crystal structures were allowed to relax during optimization.

Chemical bonding analyses on the lowest-energy structures generated from *VASP* calculations were performed on the basis of first-principles electronic band structures and magnetic moments calculated with the tight-binding linear muffin-tin orbital (TB-LMTO) method [26] by employing the non-local generalized gradient approximation (GGA) for exchange and correlation. Linear muffin-tin orbital theory [27] represents a fast, linearized form of the KKR method [28,29]. The TB-LMTO calculations were carried out within the atomic spheres approximation (ASA) [26,27]. No empty spheres were necessary to achieve space filling. The Perdew–Wang non-local exchange-correlation potential as implemented in the *LMTO* code [30] was used for the GGA calculations. A total of 255–578 irreducible *k*-points were needed for Brillouin zone integrations using the tetrahedron method [31]. Self-consistency was achieved when the total-energy change was smaller than 0.01 mRy (0.136 meV). The chemical bonding analyses were based on the density of states (DOS) and crystal orbital Hamilton population (COHP) curves [16]. COHP curves decompose the band energy into specific pairwise interatomic orbital interactions and can adopt negative (bonding), zero (non-bonding), or positive (antibonding) values.

3. Results and discussion

Structural parameters and magnetic moments were calculated using the *VASP* code for the five series $Sc_2FeRu_{5-n}Rh_nB_2$, $Sc_2CoRu_{5-n}Rh_nB_2$, $Ti_2CoRu_{5-n}Rh_nB_2$, $Ti_2FeRu_{5-n}Rh_nB_2$, and $Nb_2FeRu_{5-n}Rh_nB_2$ allowing the Rh content *n* to take the six integer values ranging from zero to five. Among the 30 different compounds under theoretical consideration, only about one-third has been either published or synthesized in our laboratories up to now. For theoretical consideration, various arrangements of Ru and Rh atoms were explored, and the lowest-energy structures based on total-energy calculations were considered for further analysis. These particular arrangements were characterized by maximum bond energy (or overlap populations), i.e., integrated COHP values, between the central *M′* atom and the surrounding Rh atoms. In addition, all structures were examined computationally for non-magnetic, ferromagnetic, or various antiferromagnetic arrangements of local moments since these compounds exhibit significant changes in magnetic responses [4]; the lowest energy arrangements for each case were subsequently analyzed. In general, non-magnetic structures are significantly disfavored energetically, and, therefore, neglected in our discussion. Within the theoretically calculated $Sc_2FeRu_{5-n}Rh_nB_2$ and $Ti_2FeRu_{5-n}Rh_nB_2$ series, respectively, those compounds which exhibit a VEC up to 62 electrons favor an antiferromagnetic arrangement, which is in perfect agreement with the experimental results (Table 1). It is important to note that the energetic differences between the antiferromagnetic and ferromagnetic states are quite subtle

Table 1
Theoretically predicted (theor., VASP-GGA) and experimentally determined [2,4,17,38] (exp., $B_0 = 5$ T at 4 K) saturation magnetic moments in Bohr magnetons (μ_B), for different compositions of the $M_2M'Ru_{5-n}Rh_nB_2$ series with $n = 0$–5 and associated valence electron counts (VEC).

VEC:		60	61	62	63	64	65	66	67	68	69
Compound											
$Sc_2FeRu_{5-n}Rh_nB_2$	Theor.	▬	▬	▬	3.55	4.07	4.30				
	Exp.	▬	▬	▬	3.0	3.1	3.3				
$Sc_2CoRu_{5-n}Rh_nB_2$	Theor.		1.86	2.15	2.47	2.71	2.84	**2.96**			
$Ti_2FeRu_{5-n}Rh_nB_2$	Theor.			▬	3.09	3.76	4.34	**4.38**	4.02		
	Exp.			**	0.6*	1.8*	2.2*	**3.1**	2.4*		
$Ti_2CoRu_{5-n}Rh_nB_2$	Theor.				1.89	2.31	2.80	**3.10**	3.06	2.63	
$Nb_2FeRu_{5-n}Rh_nB_2$	Theor.					3.40	4.07	**4.48**	4.33	4.30	3.98

*: hysteresis is not completely saturated at $B_0 = 5$ T (4 K); **: not synthesized yet; ▬: antiferromagnetic compound.

Table 2
Local orbital contributions to the saturation magnetic moment in Bohr magnetons (μ_B) as obtained from LMTO-GGA calculations.

Element	Orbital	$Sc_2CoRh_5B_2$	$Ti_2CoRu_2Rh_3B_2$	$Ti_2FeRuRh_4B_2$	$Nb_2FeRu_3Rh_2B_2$
	s	0.02	0.01	0.03	0.03
M′	*p*	0.00	0.00	0.02	0.02
	d	2.06	2.01	3.21	3.13
	s	–	0.00	0.00	−0.01
Ru	*p*	–	0.00	0.00	−0.01
	d	–	0.25	0.06	0.56
	s	−0.01	−0.01	−0.01	0.00
Rh	*p*	−0.02	−0.01	−0.01	−0.01
	d	1.10	0.70	0.99	0.60
Saturation moment μ		3.14	3.02	4.42	4.47

Magnetic moments of *M* and B atoms have been neglected.

(20.0–60.0 meV per unit cell) in the target region (VEC: 60–62 electrons). A VEC increase beyond 62 electrons stabilizes the ferromagnetic state significantly. The situation within the $Sc_2CoRu_{5-n}Rh_nB_2$ series is not as clear because a VEC between 61 and 63 electrons does not show significant energy differences between the different magnetic orderings. A shift of the VEC beyond 63 electrons stabilizes the ferromagnetic ordering. All compounds of the other series ($Ti_2CoRu_{5-n}Rh_nB_2$, $Nb_2FeRu_{5-n}Rh_nB_2$) exhibit a strong stabilization within the ferromagnetic state.

The compounds and their calculated total magnetic moments, predicted by use of the *VASP* code, as well as the experimental results, are listed in Table 1. In addition, the unit cell parameters for the lowest-energy structures of each compound are given in the supporting information (Table A); for the experimentally synthesized compounds in Table B.

As Table 1 indicates, the majority of cases exhibit its largest total magnetic moment at a VEC of 66 electrons. This trend of maximizing the total magnetic moment at 66 valence electrons is striking, even for the series $Sc_2FeRu_{5-n}Rh_nB_2$ and $Sc_2CoRu_{5-n}Rh_nB_2$, which show a steady increase up to a VEC of 65 and 66 electrons. Furthermore, the trend is independent from the chemical compositions of the compounds, in particular, with respect to the different Ru/Rh ratios, as well as the identity of the *M* (Sc, Ti, Nb) and magnetically active *M′* elements (Fe, Co). These results are in accordance with the experimentally synthesized $Sc_2FeRu_{5-n}Rh_nB_2$ series (Table 1), which revealed a clear shift from antiferromagnetic (VEC: 60–62 electrons) to a ferromagnetic ordering (VEC: 63–65 electrons). Furthermore, we see a steady increase of the total saturation moment from 3.0 μ_B (VEC: 63 electrons) up to 3.3 μ_B (VEC: 65 electrons) at 4 K and $B_0 = 5$ T, well reproduced by our theoretical results. Nonetheless, the magnitude of the theoretically determined saturation moments is slightly larger compared with the experimental ones, which can be explained by the use of GGA pseudopotentials. These are known to overestimate the structural parameters and, because of that, also the magnetic moments [32]. Note that the calculated lattice parameters are in excellent agreement with experiment (deviation $<1\%$).

Similar results are found for the $Ti_2FeRu_{5-n}Rh_nB_2$ series. The compounds with $n = 1$–3 and 5 did not reach full magnetic saturation during SQUID measurements at $B_0 = 5$ T (4 K) and, thus, the large differences between these unsaturated moments and the calculated ones are irrelevant. The theoretically determined trend, however, is correctly reproduced and, once again, shows a maximum magnetic moment for 66 valence electrons.

The calculations indicate that the saturation magnetic moments arise mainly from the 3*d* electrons of the *M′* atoms, with additional, albeit smaller, contributions from the 4*d* electrons of the Ru/Rh sites (Table 2). In contrast, the impact of the *M* atoms (Sc, Ti, Nb) and also the B atom on the total magnetic moment is evanescent.

We recall that the magnetic moment μ for a metal can be calculated according to

$$\mu = \int_{-\infty}^{\varepsilon_F} DOS^{\alpha}(E)\,dE - \int_{-\infty}^{\varepsilon_F} DOS^{\beta}(E)\,dE = N^{\alpha} - N^{\beta},$$

where N^{α} represents the number of majority spins (α) and N^{β} the number of minority spins (β) in the electronic DOS. The so-called chemical valence *Z* is simply the sum of spin-up and spin-down electrons, i.e.,

$$Z = N^{\alpha} + N^{\beta}.$$

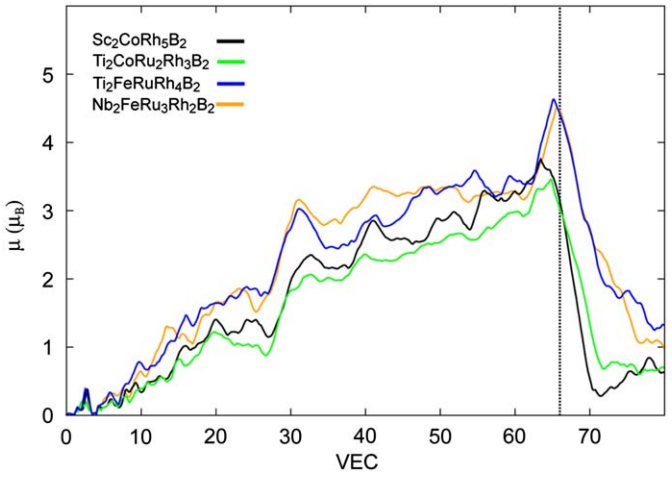

Fig. 2. Course of theoretical saturation moments obtained from spin-polarized LMTO-GGA calculations as a function of the valence electron count (VEC). The vertical dashed line marks a VEC of 66 electrons.

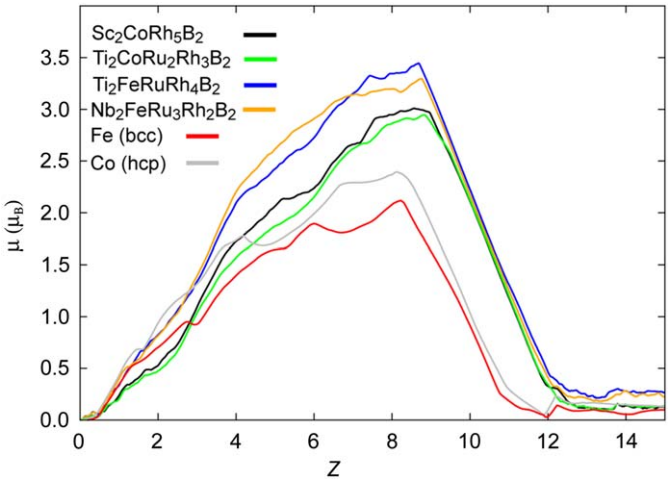

Fig. 3. Theoretically determined local magnetic moments as a function of the chemical valence at magnetically active metals from spin-polarized LMTO-GGA calculations for Co(hcp) (), Fe(bcc) (), as well as for $Sc_2CoRh_5B_2$ (; Co atoms), $Ti_2CoRu_2Rh_3B_2$ (; Co atoms), $Ti_2FeRuRh_4B_2$ (; Fe atoms), and $Nb_2FeRu_3Rh_2B_2$ (; Fe atoms). (For interpretation of the references to color in this figure legend, the reader is referred to the web version of this article.)

The magnetic moments of four selected compounds, $Sc_2CoRh_5B_2$, $Ti_2Co(Ru_2Rh_3)B_2$, $Ti_2Fe(RuRh_4)B_2$, and $Nb_2Fe(Ru_3Rh_2)B_2$, are plotted as a function of the VEC in Fig. 2. To generate these curves, the self-consistent, electronic-precise electronic structures were successively filled with a varying number of valence electrons, thereby assuming a rigid-band model. Each of these compounds has a VEC of 66 electrons, and the general shape of μ(VEC) follows a similar, volcano shape, i.e., a steady increase of μ(VEC) up to the maximum VEC, followed by a sharp drop-off of the moment beyond 66 electrons. The magnetic moments of the two Fe-containing compounds reach their maximum values exactly at a VEC of 66 electrons (Fig. 2), see also Table 1. For the Co-containing compounds, only $Ti_2CoRu_2Rh_3B_2$ shows its maximum moment at a VEC of 66 electrons, according to this rigid-band approximation, but also has a considerably smaller moment (see Table 1). $Sc_2CoRh_5B_2$, though, has its maximum moment, calculated from its electronic DOS, at a lower VEC of 63 electrons. Obviously, the rigid-band approach fails for this particular phase.

Since the total calculated magnetic moments consist mainly of the local magnetic moment of the M' (Fe or Co) atoms within the $M_2M'T_5B_2$ structure type, it is interesting to watch how this local M' contribution to the saturation moment changes while valence electrons are (computationally) added to or removed from the various structures; such a plot is shown in Fig. 3. As a reference, similar curves for Fe(bcc) and Co(hcp) are also plotted.

Just as in the preceding Fig. 2, the local moment increases with chemical valence Z up to ca. 9–10, and then it vanishes rapidly above $Z = 10$. Although Fe(bcc) has a valence of 8 and Co(hcp) has a valence of 9, both pure elements reach their highest magnetic moment at a valence of ca. 8.2. Because the magnetic moment depends on the filling of the five 3*d* orbitals and the one 4*s* orbital, there is (almost) no magnetic moment left beyond a VEC of 12.

Looking at the course of the total moments of the four complex borides, the maximum value for μ is found at $Z \approx 9$, both for the Fe- and Co-containing phases. If we assume that a rigid-band model also holds in these curves, the magnetically active transition metals must have effectively gained approximately one additional electron to achieve this critical valence, and for this particular Z, the moment of the Fe-containing phase is larger (ca. 1 μ_B) than those of the Co-phases. The behavior depicted in Fig. 3 bears a strong resemblance with what is known as Slater–Pauling curves [7,8]. If we start with the electronic structure of an intermetallic alloy that has a Fe-like valence of eight, both an increase of the electron count (say, by the partial substitution of Fe by Co) and a decrease (by the substitution of Fe by Mn) will lower the total magnetic moment.

The differences between the local magnetic moments of the magnetically most active elements and the total magnetic moment of the compound is well explained by the presence of somewhat smaller local magnetic moments at Ru and Rh sites. These moments arise because of the magnetic polarization by Co or Fe; note that neither Ru nor Rh exhibit spontaneous magnetization. Furthermore, Sc, Ti, and Nb have practically no impact on the magnetic moment, because no polarization effect, as seen for the Ru/Rh sites, is found. Only Ru/Rh form a strongly bonded nearst-neighbor coordination shell around the magnetically active elements. In addition, the early transition metals (Sc, Ti, and Nb) have only a small valence-electron count such that polarization effects are minimized. Nevertheless, these elements are still essential for adjusting the VEC in these compounds.

To get a better understanding of the chemical bonding features in the above four cases, DOS and various COHP curves were calculated. The local (or projected) DOS curves of the M' states on the basis of non-magnetic LMTO-GGA calculations are plotted in Fig. 4.

As expected, all DOS curves show major contributions of the Fe and Co 3*d* orbitals at the Fermi level. In general, no significant differences are evident, which supports the idea of similar electronic structures and magnetic behavior.

At this point, we must consider the Stoner model [33,34] for itinerant magnetism. The Stoner criterion [35,36] is a (semi-) quantitative argument for the existence of ferromagnetic ordering of the transition metals, and it can be expressed as

$$I \times N(\varepsilon_F) > 1,$$

where I is Stoner's exchange parameter, obtained from non-magnetic ground-state calculations [37] and $N(\varepsilon_F)$ is the DOS value at the Fermi level. The occurrence of ferromagnetism depends on the value of the exchange parameter, which is of the same magnitude for the magnetically active elements. Thus, large electron densities at the Fermi level are necessary in order to make $I \times N(\varepsilon_F)$ exceed unity, and this occurs whenever the

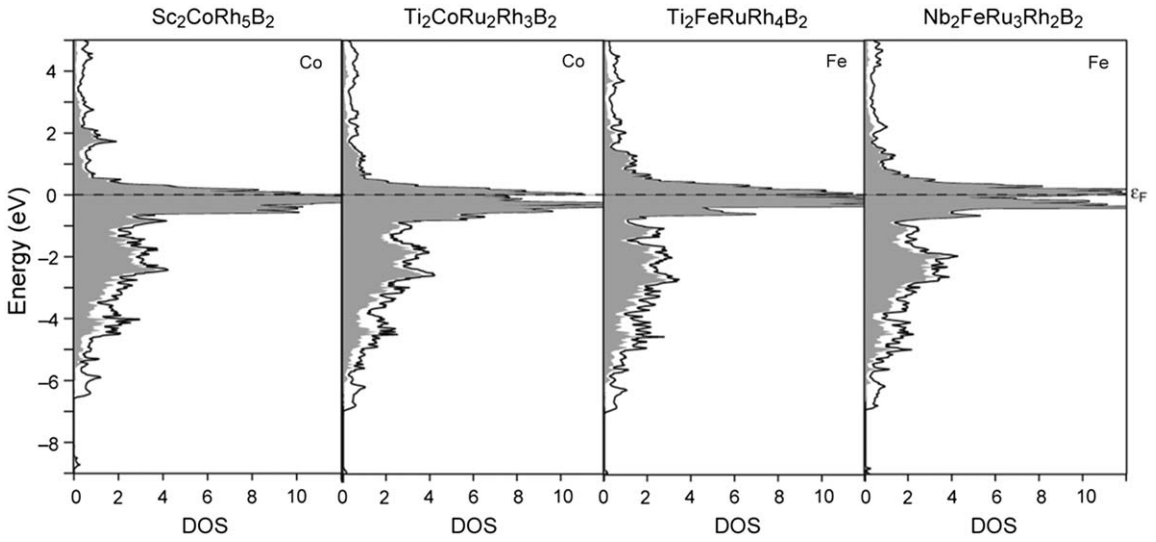

Fig. 4. Projected DOS of M' states within $M_2M'T_5B_2$ as obtained from non-spin polarized LMTO-GGA calculations. The gray part indicates M' 3*d* states.

Table 3
Number of states at the Fermi level, $N(\varepsilon_F)$, obtained from non-spin polarized LMTO-GGA calculations as well as exchange energies *I* [29] and magnetic moments obtained from spin-polarized LMTO-GGA calculations.

Compound	$N(\varepsilon_F)$ (1/eV)	*I* (eV)	$I \times N(\varepsilon_F)$	μ (μ_B)
Fe(bcc)	3.63	0.46	1.67	2.22
Co(hcp)	3.35	0.49	1.64	1.72
Ni	2.20	0.50	1.10	0.62
$Sc_2CoRh_5B_2$	7.51	0.49	3.68	3.14
$Ti_2CoRu_2Rh_3B_2$	4.43	0.49	2.17	3.02
$Ti_2FeRuRh_4B_2$	8.36	0.46	3.85	4.42
$Nb_2FeRu_3Rh_2B_2$	5.48	0.46	2.52	4.47

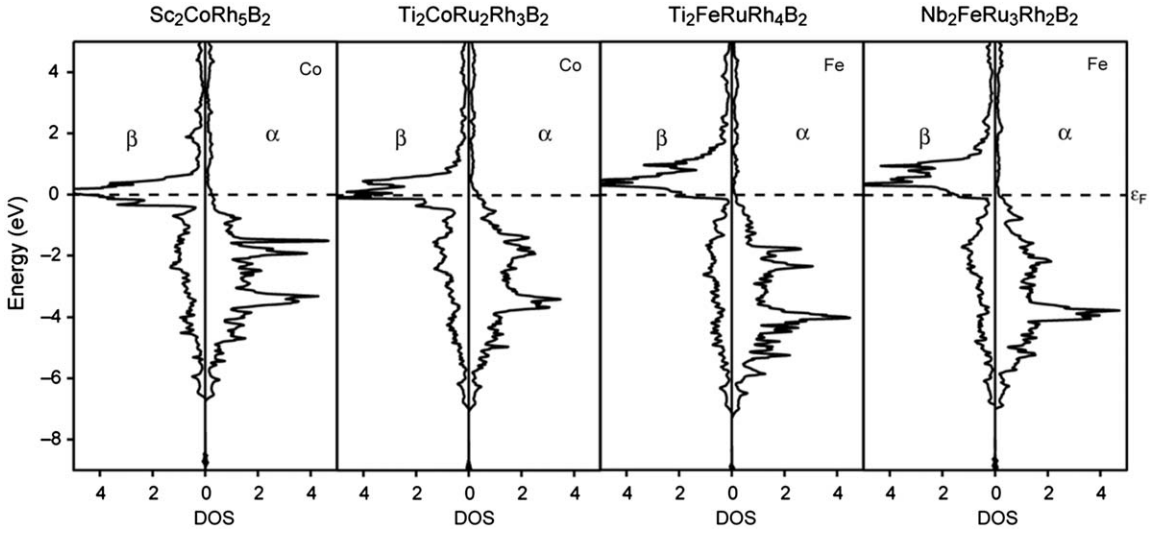

Fig. 5. Spin-polarized projected DOS of M' states within $M_2M'T_5B_2$ as obtained from LMTO-GGA calculations.

band width is small, such as for Fe, Co, and Ni. As is evident from Table 3, the theoretical results for $Sc_2CoRh_5B_2$, $Ti_2CoRu_2Rh_3B_2$, $Ti_2FeRuRh_4B_2$, and $Nb_2FeRu_3Rh_2B_2$ do fulfill the Stoner criterion, such that ferromagnetic behavior is predicted for all four compounds.

In Fig. 5, we illustrate the projected spin-polarized projected DOS curves of Co states within $Sc_2CoRh_5B_2$ and $Ti_2CoRu_2Rh_3B_2$ (VEC = 66) and Fe states within $Ti_2FeRuRh_4B_2$ and $Nb_2FeRu_3Rh_2B_2$ (also VEC = 66). Majority (α) spins are given on the right, minority (β) spins on the left.

For the projected DOS of Co (two left frames in Fig. 5), the spin density of the minority spin band at the Fermi level has a sharp peak at the top of the 3*d* band, and there is only a vanishing contribution of α states. This suggests that any electronic change

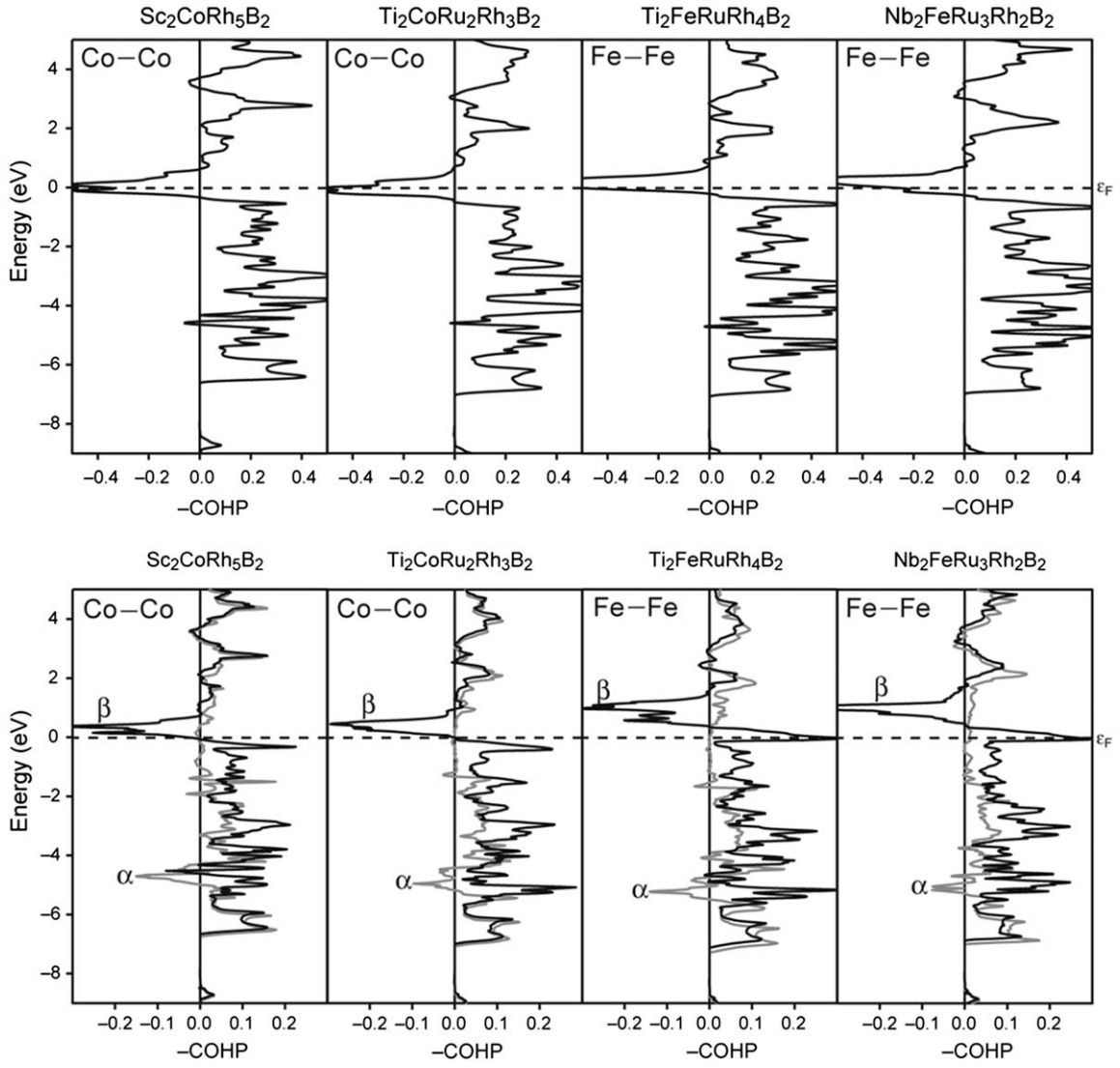

Fig. 6. Non-spin polarized (top) and spin polarized (bottom) COHP of M'–M' orbital interactions within $M_2M'T_5B_2$ as obtained from LMTO-GGA calculations.

(say, by adjusting the valence electron count) will only affect occupation of the minority spin bands. For the Fe-containing phases, the Fermi level also cuts through the minority band, but the "reservoir" of minority spins below ε_F is much smaller. Thus, similar variations of the VEC are more likely to also affect the majority spin species in the Fe-containing phases. One might therefore predict that an experimental lowering of the VEC will shift the Fermi level into the less populated spin bands, to result in either smaller saturation moments or in a completely different magnetic behavior such as antiferromagnetism.

We may also look at this phenomenon from the point of view of $M'-M'$ orbital interactions, which are projected from the DOS by COHP curves as in Fig. 6. This perspective complements the Stoner model, which identifies a potential electronic instability in the electronic DOS curve at the Fermi level by a large $N(E_F)$ value, by focusing on those $M'-M'$ interactions that promote electron transfer from one spin channel to another [39]. The net magnetic moment will be influenced by both Stoner's exchange parameter I as well as the tendency to optimize $M'-M'$ orbital interactions. Fig. 6 (top) displays an energy- and non-spin-resolved COHP analysis of $M'-M'$ bonding in the four compounds. All compounds have the Fermi level positioned within the upmost populated strongly antibonding 3*d* states of the magnetically active elements, which reflects an electronic instability of the system. The onset of spin-polarization leads to drastic changes (Fig. 6, bottom), in particular to inequivalent α and β spins. The lowering of the electronic symmetry leads to a lowering of the total and bonding energy. With regard to the majority spin channel, both Fe- and Co-containing phases have the Fermi level positioned in the non-bonding region, whereas the bonding within the Co-containing phases is optimized within the minority spins. In contrast, all bonding electrons close to the Fermi level in the Fe-containing phases belong to the minority spin channel. An experimental increase of the Fermi level into the strongly antibonding region by substitution with suitable elements destabilizes the system, thereby alluding to structural instability. A comparison between the two left and two right frames of Fig. 6 reveals, once again, that a rigid-band scenario is reasonable.

4. Conclusions

A series of complex intermetallic borides with the general composition $M_2M'T_5B_2$, in which various substitutions of metal atoms (M, M', and T) have been introduced on the basis of DFT calculations, reveals a correlation between the size of the total

(saturation) magnetic moment and the VEC. These results are analogous to the properties of the experimentally synthesized compounds, in particular, to the trend of the saturation moments, as well as the unit cell parameters. The variation of total magnetic moment with VEC by using a rigid-band approximation to the DOS of four distinct examples reveals a volcano-like, Slater–Pauling curve. The maximum magnetic moment occurs for a VEC of 66 electrons, which is nearly independent of the chemical composition. The rigid-band behavior is also observed from similar DOS and COHP curves for these phases. Because of this finding, semi-quantitative predictions have been made for several new magnetic compounds in this family, which are yet to be synthesized.

Acknowledgments

JB wants to thank Dr. German Samolyuk for helpful discussions and acknowledges Deutscher Akademischer Austauschdienst (DAAD) for financial support. The additional support by the Deutsche Forschungsgemeinschaft (DFG) and the US National Science Foundation (NSF DMR 05-02671 and 08-06507) is also gratefully acknowledged.

Appendix A. Supplementary material

Supplementary data associated with this article can be found in the online version at doi:10.1016/j.jssc.2009.07.017.

References

[1] E.A. Nagelschmitz, W. Jung, Chem. Mater. 10 (1998) 3189.
[2] E.A. Nagelschmitz, W. Jung, R. Feiten, P. Müller, H. Lueken, Z. Anorg. Allg. Chem. 97 (2001) 8617.
[3] U. Eibenstein, W. Jung, Z. Anorg. Allg. Chem. 97 (1993) 8617.
[4] R. Dronskowski, K. Korczak, H. Lueken, W. Jung, Angew. Chem. Int. Ed. 41 (2002) 2528.
[5] G.A. Landrum, R. Dronskowski, Angew. Chem. Int. Ed. 39 (2000) 1560.
[6] P. Mohn, Magnetism in the Solid State, Springer, Berlin, 2002.
[7] J.C. Slater, J. Appl. Phys. 8 (1937) 385.
[8] L. Pauling, Phys. Rev. 54 (1938) 899.
[9] W.A. Harrison, Phys. Rev. B Condens. Matter Mater. Phys. 68 (2003) 075117.
[10] C. Takahashi, M. Ogura, H. Akai, J. Phys. Condens. Matter 19 (2007) 365233.
[11] R.F. Willis, N. Janke-Gilman, Europhys. Lett. 69 (2005) 411.
[12] P. Stoch, J. Pszczola, P. Guzdek, M. Wzorek, A. Jablonska, J. Suwalski, L. Dabrowski, A. Panta, J. Alloys Compd. 384 (2004) 25.
[13] P. Stoch, J. Pszczola, P. Jagodzinski, A. Jablonska, J. Suwalski, L. Dabrowski, A. Panta, J. Alloys Compd. 384 (2004) 24.
[14] H.Z. Luo, H.W. Zhang, Z.Y. Zhu, L. Ma, S.F. Xu, G.H. Wu, X.X. Zhu, C.B. Jiang, H.B. Xu, J. Appl. Phys. 103 (2008) 083908.
[15] H. Luo, L. Ma, Z. Zhu, G. Wu, H. Liu, J. Qu, Y. Li, Phys. B Condens. Matter 403 (2008) 1797.
[16] R. Dronskowski, P.E. Blöchl, J. Phys. Chem. 97 (1993) 8617.
[17] B.P.T. Fokwa, H. Lueken, R. Dronskowski, Chem. Eur. J. 13 (2007) 6040.
[18] G.D. Samolyuk, B.P.T. Fokwa, R. Dronskowski, G.J. Miller, Phys. Rev. B 76 (2007) 94404.
[19] S. Liu, Phys. Rev. B 15 (1977) 4281.
[20] G. Kresse, J. Furthmüller, Comput. Mater. Sci. 6 (1996) 15.
[21] G. Kresse, J. Hafner, Phys. Rev. B 47 (1993) 558.
[22] P.E. Blöchl, Phys. Rev. B 50 (1994) 17953.
[23] G. Kresse, J. Joubert, Phys. Rev. B 59 (1999) 1758.
[24] J.P. Perdew, Y. Wang, Phys. Rev. B 45 (1992) 13244.
[25] H.J. Monkhorst, J.D. Pack, Phys. Rev. B 13 (1976) 5188.
[26] O.K. Andersen, O. Jepsen, Phys. Rev. Lett. 53 (1984) 2571.
[27] O.K. Andersen, Phys. Rev. B 12 (1975) 3060.
[28] J. Korringa, Physica 13 (1947) 392.
[29] W. Kohn, N. Rostoker, Phys. Rev. 94 (1954) 1111.
[30] G. Krier, O. Jepsen, A. Burkhardt, O.K. Andersen, TB-LMTO-ASA V4.7c, Max-Planck-Institut für Festkörperforschung, Stuttgart.
[31] P. Blöchl, O.K. Andersen, O. Jepsen, Phys. Rev. B 34 (1994) 16223.
[32] J.P. Perdew, in: P. Ziesche, H. Eschrig (Eds.), Electronic Structure of Solids ′91, Akademie Verlag, Berlin, 1991.
[33] E.C. Stoner, Proc. Roy. Soc. London A 154 (1936) 656.
[34] E.C. Stoner, Proc. Roy. Soc. London A 165 (1938) 372.
[35] J. Hubbard, Proc. Roy. Soc. London A 276 (1963) 238.
[36] J. Kübler, Theory of Itinerant Electron Magnetism, Clarendon Press, Oxford, 2000.
[37] J.F. Janak, Phys. Rev. B 16 (1977) 255.
[38] B.P.T. Fokwa, personal communication, Aachen, 2009.
[39] G. Samolyuk, G.J. Miller, J. Comput. Chem. 29 (2008) 2177.